



NOVA

University of Newcastle Research Online

nova.newcastle.edu.au

Mirzaeva, G.; Goodwin, G. C.; McGrath, B.; "A new understanding and improvements of finite set model predictive control in inverter applications". Published in Proceedings of the 2015 17th European Conference on Power Electronics and Applications (EPE'15 ECCE-Europe) (Geneva, Switzerland 8-10 September, 2015) (2015)

Available from: <http://dx.doi.org/10.1109/EPE.2015.7311746>

© 2015 IEEE. Personal use of this material is permitted. Permission from IEEE must be obtained for all other uses, in any current or future media, including reprinting/republishing this material for advertising or promotional purposes, creating new collective works, for resale or redistribution to servers or lists, or reuse of any copyrighted component of this work in other works.

Accessed from: <http://hdl.handle.net/1959.13/1317040>

A New Understanding and Improvements of Finite Set Model Predictive Control in Inverter Applications

G. Mirzaeva¹, G.C. Goodwin², B. McGrath³

^{1,2}The University of Newcastle, Callaghan, NSW2308, Australia

³RMIT University, Melbourne, VIC3000, Australia

E-Mails: ¹Galina.Mirzaeva@newcastle.edu.au,

²Graham.Goodwin@newcastle.edu.au

³Brendan.McGrath@rmit.edu.au

Keywords

«Converter control», «Control of drive», «Modulation strategy», «Pulse Width Modulation (PWM)», «Voltage Source Inverters (VSI)».

Abstract

This paper proposes a new interpretation of Finite Set Model Predictive Control (FS-MPC) for inverters. This interpretation gives insights into the existing limitations of FS-MPC and suggests mitigation strategies. Consequently, significant improvements of FS-MPC performance are achieved, including elimination of steady state error, improved harmonic spectrum, reduced control delays, etc. The proposed new MPC interpretation also establishes relationships between various control schemes, including FS-MPC and PWM-MPC, FS-MPC and MPC with integral action, etc. Additionally, the paper proposes further embellishments to FS-MPC based on its more efficient and accurate implementation. The findings of the paper are supported by simulations and experimental results.

Introduction

Finite Set Model Predictive Control (FS-MPC) has received considerable attention from the power electronics community in recent years. Following its early implementations for current control [1, 2] and torque control [3] of inverters, FS-MPC has been applied to a variety of converter topologies and power electronic devices [4]. One of the attractive features of FS-MPC is its simple and intuitive algorithm, with the common “core” algorithm and application specific variations.

The ideas presented in this paper will be illustrated on a common example of a current controlled voltage source inverter (VSI), which is illustrated in Fig. 1. “SV constraint” block in Fig. 1 can correspond to space vector modulation or to a finite space vector set. The three phase load shown in Fig. 1 is a typical RL network driving a three phase back-emf source.

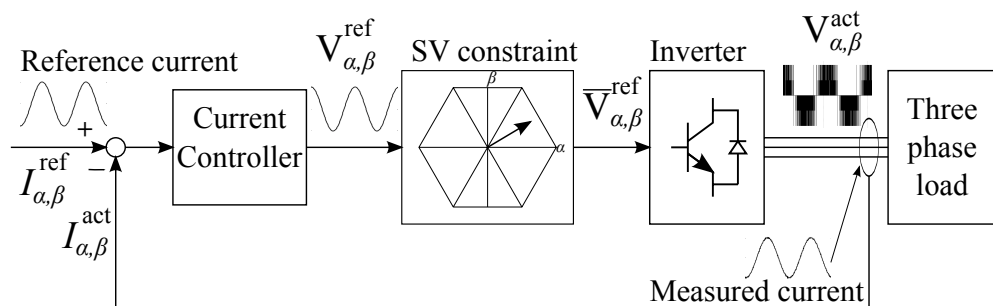


Fig. 1: A typical case of current controlled VSI driving a three phase load.

The “core” algorithm [4] of Current Control FS-MPC, horizon 1, for an RL -load with a back-emf source e , can be summarized as follows:

- Measure currents, convert into dq -frame to obtain $i_{dq}(k)$. Here we use i_{dq} to denote the vector with coordinates i_d, i_q ; k for the current time step and $k+1$ for the next step.
- For each allowable voltage vector V_{dq}^j ($j = 1, \dots, n$) drawn from a finite set \mathbf{U}^n , calculate the predicted current at $k+1$ based on the load model:

$$i_{dq}^{p,j}(k+1) = \left(1 - \frac{RT_s}{L}\right) i_{dq}(k) + \frac{T_s}{L} (V_{dq}^j - \hat{e}_{dq}(k)) = A_1 + B_1 (V_{dq}^j - \hat{e}_{dq}(k)) \quad (1)$$

where T_s is sampling period; R and L are load parameters; $A_1 = (1 - RT_s / L)$; $B_1 = T_s / L$; $\hat{e}_{dq}(k)$ is estimated back-emf.

- For each available V_{dq}^j evaluate an associated cost function which measures the error between the next step reference current $i_{dq}^*(k+1)$ and the predicted current $i_{dq}^{p,j}(k+1)$. Typical cost functions are:

$$g_1^j = \left| i_d^*(k+1) - i_d^{p,j}(k+1) \right| + \left| i_q^*(k+1) - i_q^{p,j}(k+1) \right| \quad (2)$$

$$\text{or } g_2^j = \sqrt{\left(i_d^*(k+1) - i_d^{p,j}(k+1) \right)^2 + \left(i_q^*(k+1) - i_q^{p,j}(k+1) \right)^2}$$

- Choose, from the available finite set, the voltage vector $V_{dq}^{j=m}$ which delivers the minimal cost function value $g^j = g^m$; convert into abc -frame; and apply the resulting voltage vector $v_{abc}(k+1)$ in the next control cycle.

Shortcomings of the “core algorithm” are well known. Various solutions have been proposed as outlined below:

- There is a two-step delay between the current $i_{dq}(k)$ being measured and the current resulting from application of the voltage $v_{abc}(k+1)$. This control delay may cause current oscillation around the reference. In [5] it is proposed to shift the model one step forward in time, so as to predict $i_{dq}^{p,j}(k+1)$ and modify the cost function (2) replacing $k+1$ by $k+2$.
- The number of available voltage states increases rapidly with the number of inverter levels, consequently, the amount of calculations needed at each step grows and eventually sets a limit to the control frequency and/or prediction horizon. In [6] it is proposed to reduce the allowable voltages to a subset of vectors adjacent to the vector previously applied. However, the inclusion of the optimal vector into this subset is not guaranteed.
- Apart from current control, there are other desirable properties of the control algorithm, such as low switching frequency, control of DC-link voltage, etc. Trade-offs between multiple control objectives depend on weighting coefficients in the cost function. Assigning these weights is an open problem. In [7] the researchers propose to replace the weightings by rankings, which eases the problem but does not eliminate it.
- Harmonic spectrum resulting from MPC cannot be algebraically calculated and is hard to predict. Some shaping of the MPC harmonic spectrum is reported in [8] and [9]. This is achieved by including in the cost function filtered current error or filtered voltage output, respectively.
- Under certain conditions, FS-MPC results in a non-zero steady state current error [11].

In this paper we propose a new and different interpretation of FS-MPC, which leads to novel approaches for tackling the shortcomings discussed above.

An alternative interpretation of FS-MPC

We start the discussion by replacing the commonly used approximate load model (1) by the accurate load model. It is well known that the linear RL -load in series with the back-emf source is described by a first order differential equation:

$$\frac{di_{dq}}{dt} = \frac{1}{L} (v_{dq}(t) - Ri_{dq}(t) - e_{dq}(t)) \quad (3)$$

and model (1) is obtained from (3) by using Forward Euler method of approximate integration. It has been noted in [10] that the exact solution of equation (3) can be used instead of the approximate model. The exact solution is given by:

$$i_{dq}^{p,j}(k+1) = e^{-\frac{T_s}{L/R}} i_{dq}^{p,j}(k) + \frac{1}{R} \left(1 - e^{-\frac{T_s}{L/R}}\right) \left(V_{dq}^j - \hat{e}_{dq}(k)\right) = Ai_{dq}(k) + B(V_{dq}^j - \hat{e}_{dq}(k)) \quad (4)$$

where $A = e^{-\frac{T_s}{L/R}}$ and $B = \frac{1}{R} \left(1 - e^{-\frac{T_s}{L/R}}\right)$.

Comparison between (1) and (4) reveals that in both cases the model calculations come down to one subtraction, two multiplications by pre-defined (non-integer) coefficients A and B , and a summation. It is clear that there is no computational benefit in using the Euler approximation (1). On the other hand, the introduced model inaccuracy may cause problems, particularly, with longer horizons or at lower frequencies. This is particularly important to correctly capture the sampling zeros [13]. In the remainder of this paper we will use the exact model expression (4).

We now propose a different interpretation of horizon 1 FS-MPC, which can be potentially extended to horizon > 1 . For simplicity, in the load model (3) we omit the back-emf term, which is related to mechanical speed, changes slowly and can be assumed constant over a control interval. From (4), the load model can then be written as:

$$i_{dq}(k+1) = Ai_{dq}(k) + Bv_{dq}(k) \quad (5)$$

1) Model inversion. Instead of predicting the future current values for each allowable voltage, we find the desired voltage that will bring the current to its reference value $i_{dq}^*(k+1)$ in the next control interval, using the inverse load model:

$$v_{dq}^*(k) = \frac{1}{B} \left(i_{dq}^*(k+1) - Ai_{dq}(k) \right) \quad (6)$$

2) Transformation of the cost function minimization into the voltage domain. For each allowable voltage drawn from the finite set, we calculate the cost function as the distance between the allowable voltage and the desired voltage. For the reasons explained later we prefer to express the cost function as the Euclidean norm $g = \sqrt{(\cdot)^2 + (\cdot)^2}$. Using (6), the cost function for the candidate voltages V_{dq}^j becomes:

$$g = \sqrt{\left(v_d^* - V_d^j\right)^2 + \left(v_q^* - V_q^j\right)^2} = \sqrt{\left(\frac{i_d^*(k+1) - Ai_d(k)}{B} - V_d^j\right)^2 + \left(\frac{i_q^*(k+1) - Ai_q(k)}{B} - V_q^j\right)^2} \quad (7)$$

Alternatively, if we used the traditional cost function for current (the second expression in (2)), the cost would be:

$$g_2 = \sqrt{\left(i_d^*(k+1) - i_d^{p,j}(k+1)\right)^2 + \left(i_q^*(k+1) - i_q^{p,j}(k+1)\right)^2} = \sqrt{\left[i_d^*(k+1) - (Ai_d(k) + BV_d^j)\right]^2 + \left[i_q^*(k+1) - (Ai_q(k) + BV_q^j)\right]^2} \quad (8)$$

which is identical to (7) save for scaling by the constant coefficient $B > 0$. Clearly, the cost function (7) will be minimized by exactly the same voltage V_{dq}^j that minimizes the cost function (8). The main difference of the proposed approach is that the cost function minimization is performed in the voltage domain.

Selection of the discrete voltage, which is the closest to the desired (continuous) voltage in the sense of a given criterion, is known as voltage discretization, or voltage quantization. Therefore, **horizon 1 FS-MPC comes down to model inversion followed by voltage quantization**. This is a very important notion, which explains the existing shortcomings of FS-MPC and opens new opportunities for its performance improvement, as discussed below.

Interpretation of FS-MPC as the load model inversion followed by the voltage quantizer is illustrated in Fig.2, where the inverse model is in the form given by (6) and the cost function minimization is performed by the nearest neighbour quantizer in accordance with (7). Parameters A and B are defined in (4). The circuit of Fig. 2 can be driven either by the recent $i^*(k)$ or by the predicted $i^*(k+1)$ future current reference.

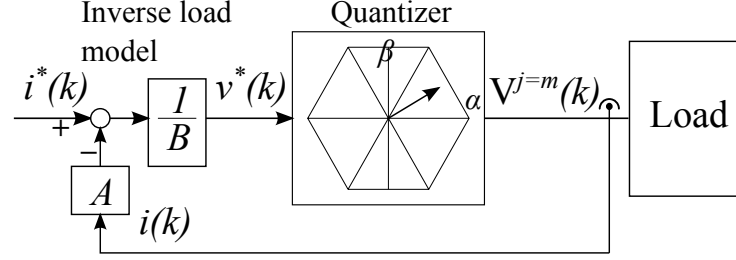


Fig. 2: Interpretation of MPC as Inverse Plant Model.

Performance limitations of the existing FS-MPC

Steady state error

Further manipulation of the inverse load model (6) yields:

$$v_{dq}^*(k) = \frac{R}{1 - e^{-\frac{T_s}{L/R}}} \left(i_{dq}^*(k+1) - e^{-\frac{T_s}{L/R}} i_{dq}(k) \right) = \frac{R}{1 - e^{-\frac{T_s}{L/R}}} \left(i_{dq}^*(k+1) - i_{dq}(k) \right) + Ri_{dq}(k) \quad (9)$$

Since $e^{-\frac{T_s}{L/R}} \rightarrow 1$, the first term in (9) constitutes a high gain applied to the current error. The gain becomes higher as the control period T_s decreases. The future value of the reference current $i_{dq}^*(k+1)$ can be predicted using various methods [1].

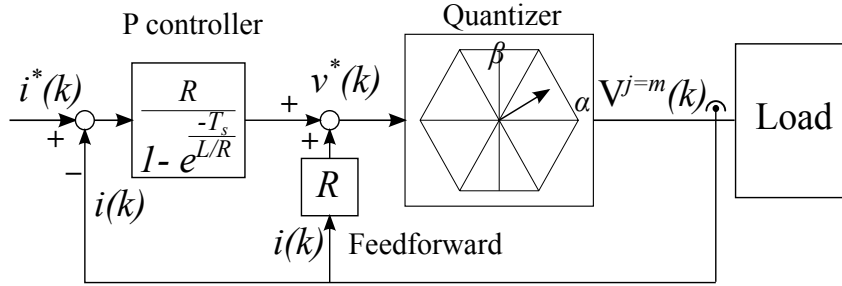


Fig. 3: Interpretation of MPC as a P-controller with feedforward.

Then FS-MPC horizon 1 given by (9) can be interpreted as a high gain Proportional Controller with feedforward compensation of the resistive voltage drop Ri , as shown in Fig.3. Clearly, such a controller would have a steady state error problem, which is a well-known problem with FS-MPC [11]. This problem can be further demonstrated by using Fig. 3 and the load model (5), along with definitions of A and B from (4), which after some manipulations yield:

$$i \approx i^* \frac{\tilde{L}e^{j\omega_0 T_s}}{(R - \tilde{R})T_s + (\tilde{L} - L) + Le^{j\omega_0 T_s}} + q \frac{T_s}{(R - \tilde{R})T_s + (\tilde{L} - L) + Le^{j\omega_0 T_s}} \quad (10)$$

where V is the actual voltage applied to the load; \tilde{R} and \tilde{L} are assumed model parameters; and q is quantization noise.

Here we use approximation $e^{-x} \approx 1 - x$ and take $z = e^{j\omega_0 T_s}$ for steady state at fundamental frequency ω_0 . Clearly, the reference tracking of FS-MPC depends on accurate knowledge of both model parameters R and L , and can be significantly corrupted due to the model errors.

Fast dynamic performance is considered to be one of the FS-MPC advantages [4]. However, in cases when there is a steady state error, dynamic performance also suffers.

Harmonic performance issues

Another known limitation of FS-MPC is limited quality of its harmonic performance [10]. Recent studies comparing performance of FS-MPC and PWM [16] have shown that FS-MPC has a comparable overall harmonic performance to that of PWM. The main limitations of the harmonic performance of FS-MPC are that the resulting spectrum: (a) is spread across a wide range of

frequencies; and (b) is random-like and unpredictable, as opposed to the discrete spectrum of PWM, which can be found analytically.

There have been some studies attempting to analytically describe the FS-MPC harmonic spectrum. For example, in [14] it has been demonstrated that the anti-windup version of FS-MPC has the form of a voltage quantizer with a feedback around it, as in Fig. 4. Indeed, using Fig. 2 and the load model (5) in Z-domain, one obtains:

$$V = \frac{1}{B}i^*z - \frac{A}{B}i + q = \frac{1}{B}i^*z - \frac{Az^{-1}}{1-Az^{-1}}V + q \Rightarrow V = \frac{1-Az^{-1}}{Bz^{-1}}i^* + q(1-Az^{-1}) = V^* + q(1-Az^{-1}) \quad (11)$$

The first term in (11) is the current reference, which is transformed via the inverse load model into the voltage reference V^* , and the second term is somewhat shaped quantization noise. It is straightforward to show that the anti-windup scheme of Fig. 4 is described by the exactly same expression: $V = V^* + q(1-Az^{-1})$. The harmonic performance of the feedback quantizer of Fig. 4 was previously studied by the authors and was found approximately similar to the performance of a sigma-delta modulator [15] save for anti-windup.

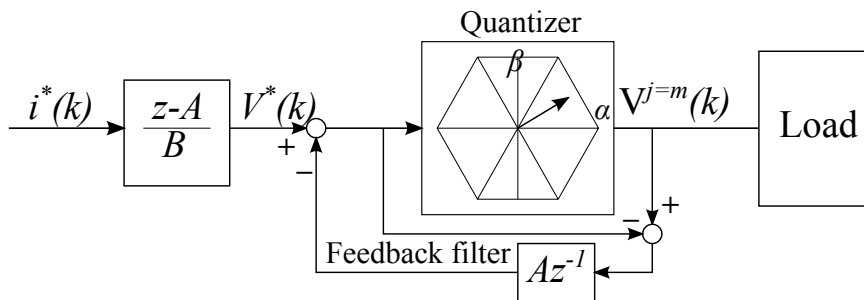


Fig. 4: Interpretation of FS-MPC as a feedback quantizer.

Performance improvements of FS-MPC based on the new interpretation

The new interpretation of FS-MPC proposed in this paper and the new insights illustrated by Figs. 2-4 assist in developing the most effective strategies to overcome the limitations listed above and other shortcomings of the traditional FS-MPC.

Elimination of steady state error

In our earlier discussion, the inverse model based controller, which is equivalent to the traditional FS-MPC, has been found sensitive to parameter errors. A straightforward way to achieve zero steady state current error is using a more appropriate controller: a PI controller if control is performed in rotating frame; or a Proportional + Resonant (PR) controller if control is performed in stationary frame. Fig. 5 shows the diagram corresponding to the latter case with the PR controller implemented.

Optimization of the controller parameters with respect to the tracking performance has been presented in [17]. It has been shown that the optimal tracking performance is achieved if:

- In case of a PI controller $K_p = B$ (defined in (4)) and $\tau_i = L/R$;
- In case of PR controller $K_p = B$, $\tau_i = L/R$, and resonance damping $\beta = 0.9 \dots 0.99$.

Improvement of harmonic performance (achieving a discrete spectrum)

The interpretation of MPC current control as an inverse plant model followed by a quantizer suggests that the harmonic performance can be altered if a different type of quantizer is being used to approximate the voltage $v_{dq}^*(k)$ obtained from the model inversion (6). Various quantizer options include (but are not limited to):

- Nearest neighbor quantizer which chooses only one voltage state for the entire duration of the control period. If this type of the quantizer is chosen then the typical FS-MPC [4] results;

- A sequence of voltage pulses with equal duration so chosen that the desired voltage $v_{dq}^*(k)$ is approximated as close as possible. If this type of the quantizer is chosen then a hybrid MPC with switching pattern results, which is explained, for example, in [18];
- A sequence of voltage pulses with the calculated durations so chosen that the desired voltage $v_{dq}^*(k)$ is achieved exactly, in both magnitude and phase. If this type of the quantizer is chosen then PWM implementation of MPC (or PWM-MPC) results, which is becoming increasing popular in power electronics [19].

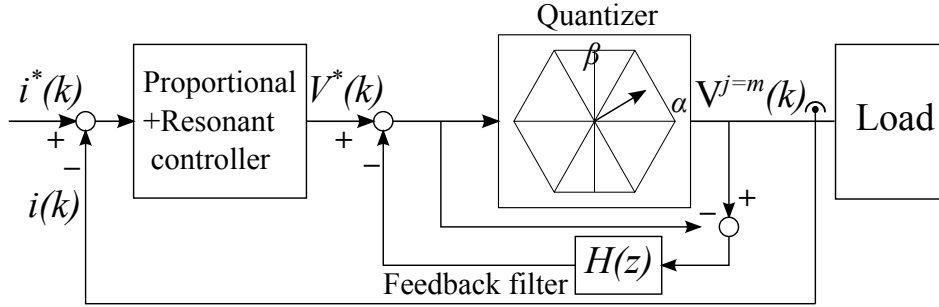


Fig. 5: Improved version of FS-MPC with a PR controller

Improvement of harmonic performance (shaping of the inverter quantization noise)

The authors have previously extensively studied noise shaping strategies for feedback quantizer (see, for example [12]). In this paper we have established the connection between FS-MPC and feedback quantizer, which makes all those noise shaping strategies applicable to FS-MPC. In the diagram of Fig. 5 noise shaping is performed by a feedback filter $H(z)$, which can be designed to meet the given criteria. For instance, it can eliminate a particular frequency component causing resonance; or a number of selected frequency components; or it can significantly reduce a particular range of frequencies. We refer the reader to [12] for the details of the feedback filter design.

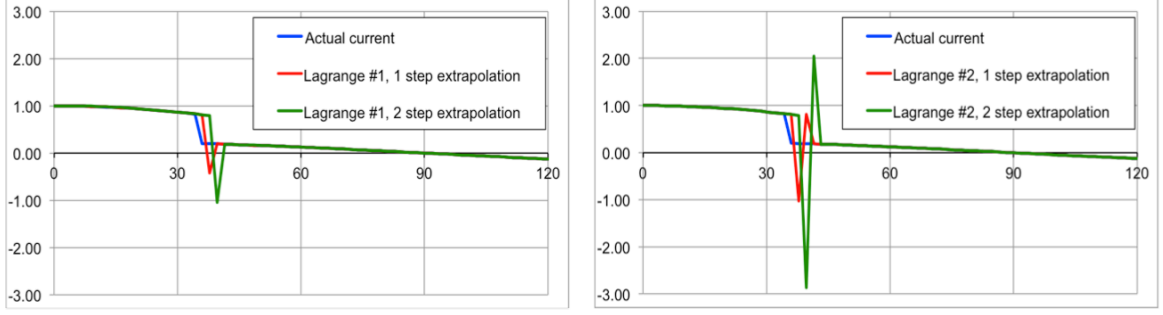
Note that the additional feature of shaping the inverter quantization noise can be used in combination with any modulation strategy explained in the previous subsection. For example, the distributed inverter noise spectrum produced by FS-MPC can be shaped so that particular spectral components or frequency ranges are mitigated. Or, the discrete inverter noise spectrum produced by PWM-MPC can be additionally shaped as to achieve a desired variation of its properties.

Compensation of the transport delay

As explained in [6], typically FS-MPC has a delay of two control cycles between the current measurement and the effect seen in the current as the result of control action. The effect of this delay is twofold. Firstly, it causes the current produced by FS-MPC to oscillate around its set point [6], which is the manifestation of instability.

Secondly, even if the transport delay is accounted for, for example, by shifting the prediction model one step forward in time [6], then there is still a two-step delay between the current reference $i^*(k)$ which drives the circuits of Figs. 2-4, and the output load current. One suggestion to eliminate this delay [6] is to drive the control circuits of Figs. 2-4 by $i^*(k+2)$ predicted using Lagrange polynomial interpolation.

The authors studied Lagrange polynomial interpolation and found out that it works well in steady state but causes unacceptable transients if the reference current undergoes rapid changes. The latter is illustrated in Fig. 6 and Table I. Linear and quadratic Lagrange polynomial interpolations were calculated and then extrapolated one and two steps forward, resulting in expressions given in Table I. These extrapolations were then applied to a sine wave, the amplitude of which dropped from 100% to 25% at $\theta = 36^\circ$, simulating a sudden change in the required torque. As can be seen from Fig. 6 and Table I, under such conditions the extrapolated signals undergo severe disturbances, potentially causing stability problems of the control loops.



a) 1st order Lagrange polynomial;

b) 2nd order Lagrange polynomial.

Fig. 6: Extrapolation of Lagrange interpolation polynomials under sudden current step change.

Table I: Expressions for extrapolated Lagrange polynomials one and two steps forward

| | $i^{ext}(k+1)$ | $i^{ext}(k+2)$ | Max. disturbance, % | |
|-------------------------|----------------------------|-----------------------------|---------------------|------|
| Linear interpolation | $2i(k) - i(k-1)$ | $3i(k) - 2y(k-1)$ | 62% | 124% |
| Quadratic interpolation | $3i(k) - 3i(k-1) + y(k-2)$ | $6i(k) - 8i(k-1) + 3y(k-2)$ | 123% | 306% |

The authors propose a novel and very effective approach to account for and compensate for the transport delay associated with either FS or PWM implementations of MPC. This approach is based on using a generalized MPC framework in combination with Internal Model principle, and is described in detail in [20].

The appropriate plant model and (importantly) the appropriate reference and disturbance models form the basis of such optimal controller design. The design described in [20] automatically results in an anti-windup form of the optimal controller with respect to tracking the modeled reference and rejecting the modelled disturbance. The transport delay is compensated for provided that it is included in the plant model.

Fig. 7 present the resulting structure and parameters of the optimal controller with respect to tracking constant references and rejecting constant disturbances, with transport delay compensation. Fig. 8 presents the resulting optimal controller for sinusoidal reference tracking and sinusoidal disturbance rejection, with transport delay compensation. The properties of these controllers are studied in [17].

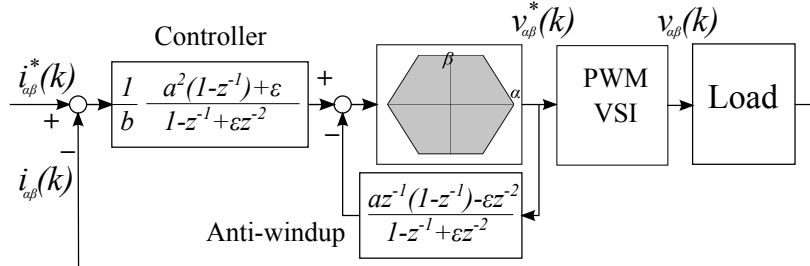


Fig. 7: Optimal MPC (extended PI) controller for constant reference and disturbance.

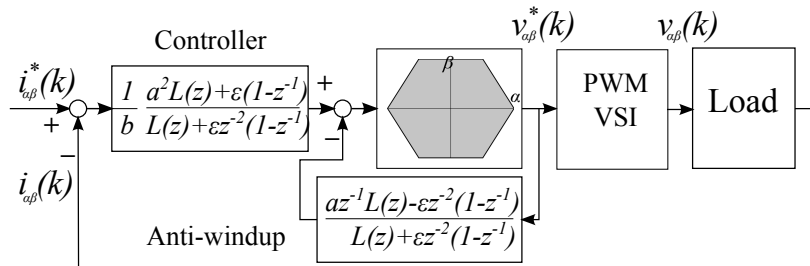


Fig. 8: Optimal MPC (extended PR) controller for sinusoidal reference and disturbance.

Additional embellishments of FS-MPC

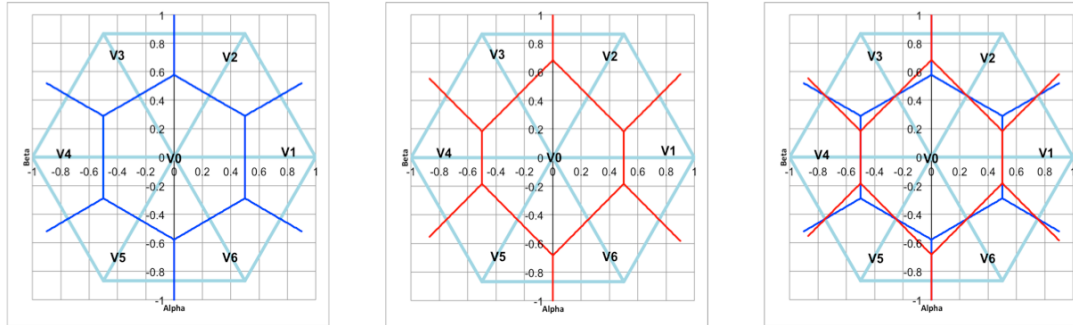
Reduced amount of calculations

In the current domain, the cost function must be calculated in each control cycle, according to (8), for all space vectors that produce different voltages: 7 vectors for 2-level inverters; 19 vectors for 3-level inverters, etc. The required amount of calculation is significant and grows rapidly with the number of inverter levels. There exist techniques to reduce the number of candidate vectors to some subset [6] but they do not guarantee that the optimal voltage vector is always included in this subset.

If the cost function is calculated in the voltage domain as proposed, it can be calculated in each control cycle for only 3 voltage vectors nearest to the desired vector, for any number of inverter levels, without any risk to miss the best voltage. The amount of calculations is reduced significantly, namely, to 3/7 for 2-level inverters, to 3/19 for 3-level inverters, etc. This may open the door to use longer prediction horizons for multi-level inverters, which at the moment is limited by processor computational power. A further small reduction in the required calculations comes from the fact that the load model is applied only once in (6), rather than for each V_{dq}^j of the finite set as in (8).

Equal utilization of all active space vectors

As mentioned earlier, FS-MPC uses the cost function in the form of the Euclidean norm or the sum of the moduli (refer to the two expressions in (2)). The latter is more common due to the apparent computational benefit. However, voltage mapping based on the Euclidean norm results in an equal utilization of all active space vectors, while voltage mapping based on the sum of the moduli underutilizes vectors V1 and V4, which is illustrated in Fig. 9. In the voltage domain, comparison between the Euclidean norms is greatly simplified and does not require any non-linear operations. For example, the square of distance from the desired v_{dq}^* to the space vector V1 yields:



a) Distance as $\sqrt{a^2 + b^2}$; b) Distance as $|a| + |b|$; c) Difference between a) and b).

Fig. 9: Mapping of an arbitrary voltage vector to vectors from Finite Set for 2-level inverter.

$$D_1^2 = (v_d^* - 1/2)^2 + (v_q^* - \sqrt{3}/2)^2 = (v_d^*)^2 + (v_q^*)^2 + 1 - v_d^* - \sqrt{3}v_q^* \quad (9)$$

The first three terms of the result will be the same for any space vector from the finite set. Hence, for distance comparison, only the last two terms are required. Therefore, the superior distance calculation comes at no cost.

Simulation and experimental results

A large amount of simulation and experimental results have been obtained to support the findings of the paper. Only some of this data are included here. Fig. 10 shows simulated line currents and one of the line-to-line voltages for MPC controlled inverter with PWM. The detailed inverter simulation was performed using PSIM. The inverter is driving a three phase load with $L=15\text{mH}$, $R=0.1\Omega$ and back-emf 80V at 50Hz. The inverter parameters are: DC-link voltage 300V, modulation frequency 5kHz and sampling period $\Delta = 100 \mu\text{s}$.

In the case illustrated by Fig. 10a the transport delay was not compensated for. This manifests itself in a clearly seen constant delay between the reference (black) and the actual (red) line current. Fig. 10b

corresponds to implementation of the circuit shown in Fig. 8, i.e. PWM-MPC designed for sinusoidal reference and sinusoidal disturbance (aka extended PR controller) with transport delay compensation. One observes from Fig. 10b that the aforementioned delay is fully compensated for in steady state. The transient delay is inevitable since there is no way to predict when the step change of the current occurs. The transition of the current from one reference to another is performed in a very fast and smooth manner.

Fig. 11 shows experimental results corresponding exactly to the simulation results of Fig. 10b. The inverter was controlled using a TMS320F2810 fixed point DSP that was programmed to implement all inverter modulation, current regulation, protection and supervisory functions. The experimental traces closely follow the corresponding simulation results.

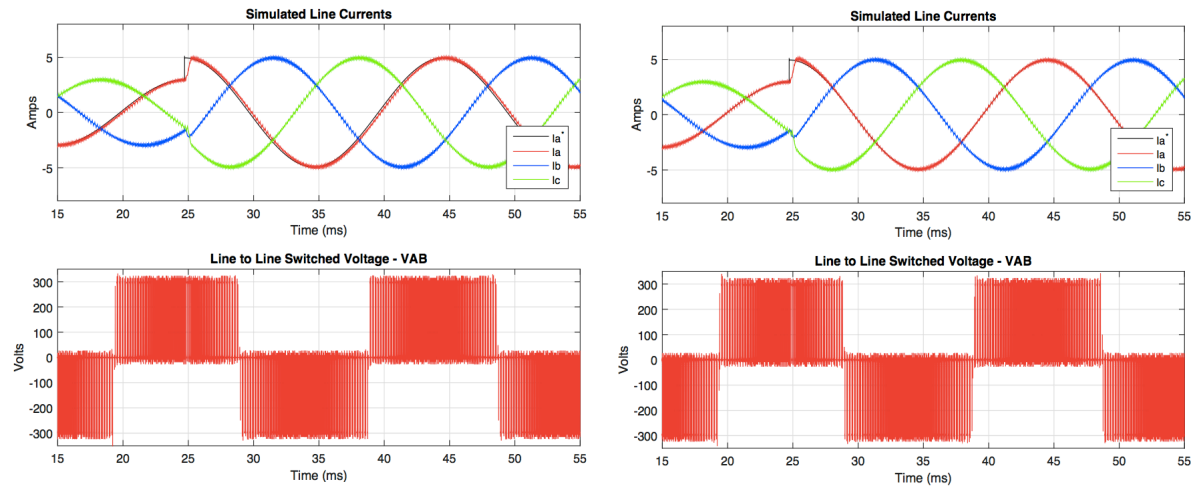


Fig. 10: Simulation results for PWM-MPC: (a) no compensation; (b) delay compensation.

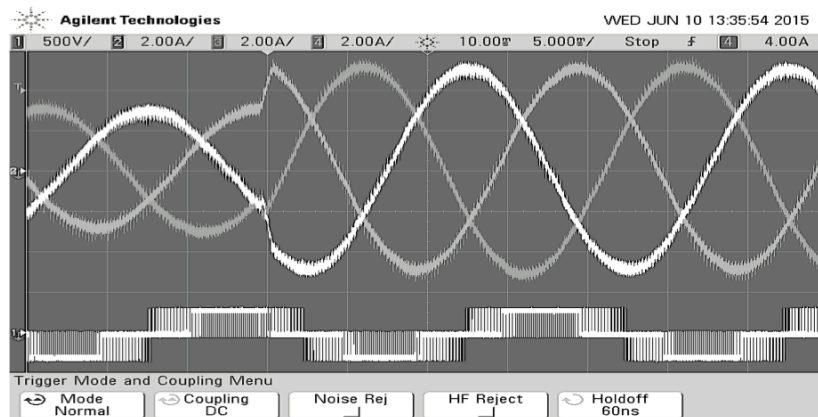


Fig. 11: Experimental results corresponding to Fig.10 (b)

Conclusion

The most important contribution of the paper is the interpretation of MPC as the plant model inversion followed by a quantizer.

Such an interpretation allows one to see clear relationships between different control schemes. For example, FS-MPC and PWM-MPC correspond to different variants of the quantizer (nearest neighbor or PWM, respectively). Proportional controller with feedforward, PI and PR controllers are different forms of the plant model inversion in the presence of certain types of disturbances.

The proposed interpretation of MPC also automatically leads to a strategy of both FS-MPC and PWM-MPC performance improvement, which is based on the inclusion of the disturbance models and transport delays in the design of the inverse plant model. Additionally, some further embellishments to the FS-MPC implementation are proposed, resulting in reduced calculation time and better space vector utilization. The findings of the paper are supported by simulation and experimental results.

References

- [1] J. Rodriguez, J. Pontt, C. Silva, M. Salgado, S. Rees, U. Ammann, P. Lezana, R. Huerta, and P. Cortes, "Predictive control of three-phase inverter," *Electronics Letters*, vol. 40, no. 9, pp. 561–563, 2004.
- [2] A. Linder and R. Kennel, "Direct model predictive control - a new direct predictive control strategy for electrical drives," in *Power Electronics and Applications, 2005 European Conference on*, 2005, pp. 1–10.
- [3] H. Miranda, P. Cortes, J. Yuz, and J. Rodriguez, "Predictive torque control of induction machines based on state-space models," *Industrial Electronics, IEEE Transactions on*, vol. 56, no. 6, pp. 1916–1924, 2009.
- [4] J. Rodriguez, M. Kazmierkowski, J. Espinoza, P. Zanchetta, H. Abu-Rub, H. Young, and C. Rojas, "State of the art of finite control set model predictive control in power electronics," *Industrial Informatics, IEEE Trans. on*, vol. 9, no. 2, pp. 1003–1016, 2013.
- [5] P. Cortes, J. Rodriguez, C. Silva, and A. Flores, "Delay compensation in model predictive current control of a three-phase inverter," *Industrial Electronics, IEEE Transactions on*, vol. 59, no. 2, pp. 1323–1325, 2012.
- [6] P. Cortes, A. Wilson, S. Kouro, J. Rodriguez, and H. Abu-Rub, "Model predictive control of multilevel cascaded h-bridge inverters," *Industrial Electronics, IEEE Transactions on*, vol. 57, no. 8, pp. 2691–2699, 2010.
- [7] C. Rojas, J. Rodriguez, F. Villarroel, J. Espinoza, C. Silva, and M. Trincado, "Predictive torque and flux control without weighting factors," *Industrial Electronics, IEEE Transactions on*, vol. 60, no. 2, pp. 681–690, 2013.
- [8] P. Cortes, J. Rodriguez, D. Quevedo, and C. Silva, "Predictive current control strategy with imposed load current spectrum," *Power Electronics, IEEE Transactions on*, vol. 23, no. 2, pp. 612–618, 2008.
- [9] M. Perez and J. Rodriguez, "Predictive frequency spectrum shaping of currents in a three phase inverter," in *Sensorless Control for Electrical Drives and Predictive Control of Electrical Drives and Power Electronics (SLED/PRECEDE)*, 2013 IEEE International Symposium on, 2013, pp. 1–5.
- [10] P. Stolze, M. Kramkowski, T. Mouton, M. Tomlinson, and R. Kennel, "Increasing the performance of finite-set model predictive control by oversampling," in *Industrial Technology (ICIT), 2013 IEEE International Conference on*, 2013, pp. 551–556.
- [11] R. Aguilera, P. Lezana, and D. Quevedo, "Finite-control-set model predictive control with improved steady-state performance," *Industrial Informatics, IEEE Transactions on*, vol. 9, no. 2, pp. 658–667, 2013.
- [12] G. Mirzaeva and G. Goodwin, "The use of feedback quantizer PWM for shaping inverter noise spectrum," in *Power Electronics and Motion Control Conference (EPE/PEMC), 2012 15th International*, pp. 1–7, 2012.
- [13] G. Goodwin, J. Agüero, M. Cea Garridos, M. Salgado, and J. Yuz, "Sampling and sampled-data models: The interface between the continuous world and digital algorithms," *Control Systems, IEEE*, vol. 33, no. 5, pp. 34–53, 2013.
- [14] G. Mirzaeva and G. Goodwin, "Harmonic suppression and delay compensation for inverters via variable horizon nonlinear model predictive control", *International Journal of Control*, 2014, <http://dx.doi.org/10.1080/00207179.2014.948915>
- [15] G. Mirzaeva and G. Goodwin, "Feedback quantizer versus sigma-delta modulator for voltage source inverters", in *Proceedings of IECON-2012 – 38th Annual Conference of IEEE Industrial Electronics Society*, Harmonic suppression and delay compensation for inverters via variable horizon nonlinear model predictive control", 2012, pp.5938-5943.
- [16] H.A.Young, M.A.Perez, J.Rodriguez, J. and H.Abu-Rub, "Assessing Finite-Control-Set Model Predictive Control: A Comparison with a Linear Current Controller in Two-Level Voltage Source Inverters," *Industrial Electronics Magazine, IEEE*, no. 8, pp. 44–52, 2014.
- [17] G.Mirzaeva, G.C.Goodwin, B.McGrath, "Optimal Design of VSI Current Controllers based on MPC Approach", in *Proceedings of ISIE-2015 – International Symposium on Industrial Electronics*, Buzios, Rio de Janeiro, Brazil, pp.1-6. 2015.
- [18] S.Vazquez, A.Marquez, R.Aguilera, D.Quevedo, J.I.Leon, and L.G.Franquelo, "Sampling and sampled-data models: The interface between the continuous world and digital algorithms," *Industrial Electronics, IEEE Transactions on*, no. 62, pp. 2010–2010, 2015.
- [19] L.Tarisciotti, P.Zanchetta, A.Watson, P.Wheeler, S.Bifaretti and J.Clare, "Multi-objective modulated model predictive control for a multilevel solid state transformer", *Industry Applications, IEEE Transactions on*, v.PP, issue 99, pp.1-1, 2015.
- [20] G.Mirzaeva, G.C.Goodwin, B.McGrath, C.Tuxeiro, and M.Rivera, "Predictive Optimal Switching Sequence Direct Power Control for Grid-Connected Power Converters", submitted for publication in *Transactions on Industrial Electronics: Special Section on Predictive Control*, IEEE, 2015.